ACS Sustainable Chemistry & Engineering

Research Article

pubs.acs.org/journal/ascecg

Effects of Pore Structure on Performance of An Activated-Carbon Supercapacitor Electrode Recycled from Scrap Waste Tires

Mingjia Zhi,[†,‡] Feng Yang,[§] Fanke Meng,[‡] Minqi Li,[§] Ayyakkannu Manivannan,[‡,∥] and Nianqiang Wu*[,‡]

[†]Department of Materials Science & Engineering, Zhejiang University, Hangzhou 310027, China

[‡]Department of Mechanical and Aerospace Engineering and [§]Industrial and Management Systems Engineering Department, West Virginia University, Morgantown, West Virginia 26506, United States

[∥]National Energy Technology Laboratory, US Department of Energy, 3610 Collins Ferry Road, Morgantown, West Virginia 26507, United States

Supporting Information

ABSTRACT: It is important to address the challenges posed with the ever-increasing demand for energy supply and environmental sustainability. Activated carbon, which is the common material for commercial supercapacitor electrodes, is currently derived from petroleum-based precursors. This paper presents an effective synthetic method that utilizes waste tires as the precursor to prepare the activated carbon electrodes by the pyrolysis and chemical activation processes. Adjusting the activation parameters can tailor multiple physical properties of the resulting activated carbon, which in turns tunes the performance of the activated carbon electrode. Statistical multiple linear regression and stepwise regression methods are employed to investigate the dependence of the specific capacitance and the rate capability upon the physical properties (such as porosity) of the activated carbon electrode. The specific capacitance of activated carbon electrode is controlled by the micropore volume but independent of the mesopores volume. The rate capability is dominated by the mesopore/micropore volume ratio instead of the absolute value of mesopore volume.

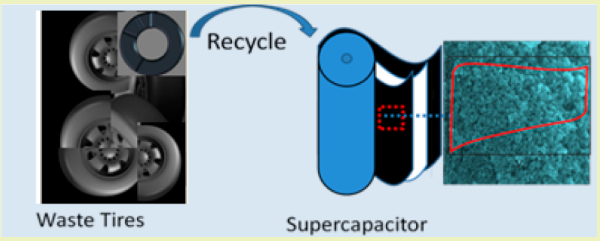

KEYWORDS: *Activated carbon, Waste tire, Supercapacitor, Electrode, Porous material*

INTRODUCTION

A supercapacitor is an energy storage device that has found increasing application in renewable energy power plants, hybrid electric vehicles, and large industrial equipment.[1−5] Commercial supercapacitors are designed based on electric double-layer capacitance (EDLC), and their electrodes are made of porous activated carbon. In addition, researchers are developing pseudocapacitors in which activated carbon serves as the support backbone for pseudocapacitive materials.[4−8] Currently petroleum-derived coke, pitch, and coal are the common precursors for production of commercial activated carbon.[9−11] The decreasing availability of fossil-based carbon compounds has driven the industry to search for sustainable resources to synthesize activated carbon. For example, activated carbon has been produced from renewable biomass precursors such as sucrose, cellulose, corn grains, sugar cane bagasse, and others.[12,13]

Recycling of waste products for synthesis of activated carbon-based supercapacitor electrodes has attracted increasing attention recently.[14,15] Actually many waste products such as that of newspaper, wood, and tires are potential sources of activated carbon. For example, approximately 290 million scrap tires are generated each year in the United States. About 27 million scrap tires are disposed annually in landfills or monofills.[16] These tires are among the largest and most problematic sources of waste because they are nonbiodegradable and have a long life. Therefore, it is significant to generate useful products from waste tires. Today some waste tires are ground into crumb rubber for highway construction or ground cover. Some waste tires are recycled to produce the activated carbon that is used as environmental adsorbent for pollutant removal.[17−22] The price of general-purpose granular activated carbon ranges from $1.65 to $9.90 per kilogram in the USA[23] while the price of activated carbon used for supercapacitors is about $50/kg.[24] Therefore, it is very attractive to recycle waste tires to produce activated carbon for supercapacitor applications as a high value product. In fact, waste tires could be an attractive precursor for activated carbon. Table 1 gives the costs

Table 1. Sustainable Precursors for Activated Carbon

raw materials	cost	carbon yield
wood	$0.8/kg	25%
sucrose	$0.25/kg	<45%
coconut shell	$0.25/kg	30%
waste tire	$1 per tire or ~$0.06/kg	~30%

Special Issue: Sustainable Nanotechnology 2013

Received: February 16, 2014
Published: June 2, 2014

and the carbon yields of different precursors that are used for production of activated carbon.[12] It can be seen that waste tires have the lowest cost and moderate carbon yield as well as highest economic feasibility.

It is worth noting that the required pore structure of activated carbon for supercapacitors is totally different from that for environmental absorbents. Therefore, although some synthesis methods have been developed for production of waste tire-derived activated carbon as environmental absorbents, a different synthetic route has to be explored for application in supercapacitors. This paper presents an effective synthetic route to prepare activated carbon from the recycled waste tires for use in supercapacitor electrodes. The porosity and other physical properties may have a significant effect on the specific capacitance and the rate capability of the supercapacitor made of activated carbon. In particular, both mesopores and micropores in activated carbon play important roles in the electrochemical behaviors of EDLC-based supercapacitors. Therefore, the activation condition will be optimized in order to tune the specific surface area, the mesopores, and the micropores.

In order to guide the design of materials for an EDLC-type supercapacitor electrode, it is imperative to unravel the correlation between the specific capacitance and the rate capability of the activated carbon electrode and its physical properties such as the specific surface area, total pore volume, micropore volume, and mesopore volume. Herein statistical modeling methods such as multiple linear regression and stepwise regression are employed to investigate the impacts of multiple factors in a statistically valid manner.

EXPERIMENTAL SECTION

Material Synthesis. The waste tire-derived activated carbon (WTAC) was prepared by the pyrolysis and activation processes as shown in Scheme 1. A piece of cleaned scrap waste tire was loaded into a quartz tube furnace and pyrolyzed in N_2 atmosphere at 600 °C for 3 h. The resulting char was ground to powder and washed with a 1 M HCl solution to remove the metallic impurities and sulfur, followed by washing with water several times and then dried in vacuum at 120 °C for 12 h. Subsequently, the char was mixed with H_3PO_4 powder and activated in nitrogen at a given temperature for different time intervals. Both the heating and the cooling rates were 5 °C/min. The activated carbon was then washed with water several times until the pH value of the filtered liquid reached about 7. To investigate the correlation of the specific capacitance and the rate capability of activated carbon electrode with its physical properties, various activation experiments were performed following the central composite design, a commonly used design method for nonlinear models, as shown in Table 2.

Scheme 1. Flow Chart Showing the Preparation of Activated Carbon with Waste Tire As the Precursor

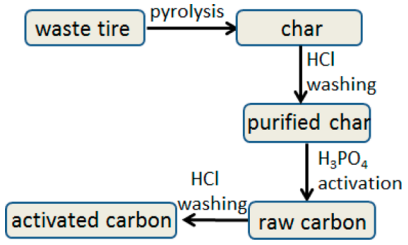

Materials Characterization. The morphology of the as-prepared activated carbon was observed by with a JEOL field-emission scanning electron microscope (FE-SEM, JEOL 7600). The specific surface area and the pore size distribution of activated carbon were measured by N_2 adsorption at 77 K using a Micromeritics ASAP 2020 analyzer.

Table 2. Experimental Details of Activation of Waste Tire-Derived Char

sample ID	H_3PO_4/char (mass ratio)	activation temperature (°C)	activation time (h)
WTAC-1	6	840	2.4
WTAC-2	9	840	2.4
WTAC-3	6	960	3.6
WTAC-4	9	960	2.4
WTAC-5	9	960	3.6
WTAC-6	7.5	900	2
WTAC-7	7.5	900	4
WTAC-8	7.5	900	3
WTAC-9	4	900	3
WTAC-10	4.4	870	3.3
WTAC-11	4.4	930	2.7
WTAC-12	5	840	3
WTAC-13	4.4	930	3.3
WTAC-14	6	900	3
WTAC-15	4.4	870	2.7
WTAC-16	5	900	3.5

Electrochemical Testing. The resulting activated carbon powder was mixed with the polyvinylidene fluoride (PVDF) binder in mass ratio of 9:1 and dispersed in the *N*-methyl-2-pyrrolidone (NMP) solvent to form a slurry. The slurry was then pasted onto Ni foil and dried at 120 °C in vacuum to form an electrode. The mass loading of the electrode was about 1 mg/cm^2. Electrochemical tests were performed on a three-electrode cell with 6 M KOH aqueous solution as the electrolyte. The activated carbon served as the working electrode, and a Pt foil and the Ag|AgCl acted as the counter and reference electrodes, respectively. Cyclic voltammetry (CV) was scanned from 2 to 200 mV/s. Galvanostatic charge−discharge experiment was performed with a specific current from 0.2 to 20 A/g. Electrochemical impedance (EIS) spectra were acquired from 30 kHz to 0.01 Hz with an open circuit at an AC amplitude of 10 mV. The EIS spectra were analyzed by the Cview and Zview software. All the data were recorded by Solartron 1287 potentiostat and Solartron 1260 impedance/grain−phase analyzer.

RESULTS AND DISCUSSION

Figure 1 shows the SEM images of the typical activated carbon (WTAC-16). The sample contained large particles in size of several micrometers (Figure 1a). The surface of particles was very rough. The close view of a single large particle reveals that the individual particles were composed of interconnected carbon nanospheres in the size of 100−200 nm (Figure 1b). The voids (macropores) formed by interconnected carbon nanospheres offered sufficient reservoirs for electrolyte, which was desirable for a supercapacitor electrode.

The N_2 adsorption−desorption experiments were performed on the activated carbon samples. Supporting Information Figure S1a shows the representative isotherm adsorption−desorption curves of the samples (WTAC-2, 3, 5, 9, and 16). All the isotherm curves showed an intermediate behavior between types I and II, which indicated that the as-synthesized activated carbon possessed both micropores and mesopores.[25] The step line at the low pressure region suggested the presence of a large fraction of micropores while the hysteresis loop at the high pressure indicated the mesoporous structure. It has also been found that the majority of pores in the sample were micropores (less than 2 nm in size). Detailed analysis of the micropore structure can be found in Supporting Information

dx.doi.org/10.1021/sc500336h | ACS Sustainable Chem. Eng. 2014, 2, 1592−1598

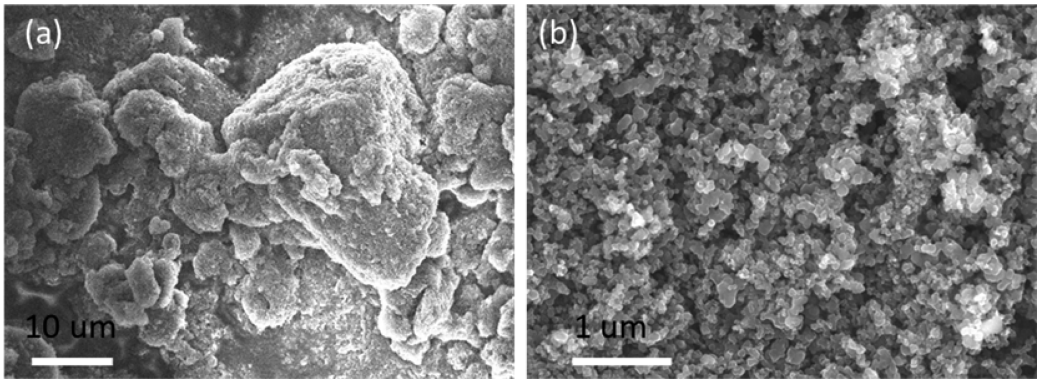

Figure 1. SEM images of the activated carbon powder (WTAC-16): (a) low-magnification image and (b) high-magnification image.

Table 3. Physical Properties and Electrochemical Performance of the Activated Carbon Electrodes

sample ID	surface area (m^2/g)	total pore volume (cm^3/g)	micropore volume (cm^3/g)	mesopore volume (cm^3/g)	micropore median size (nm)	specific capacitance (C_S) (F/g)	rate capability (R)
variable	X_1	X_2	X_3	X_4	X_5	C_S	R
WTAC-1	208.5	0.082	0.064	0.018	0.55	42.9	0.784
WTAC-2	202.5	0.066	0.058	0.007	0.52	30.6	0.607
WTAC-3	315.2	0.139	0.109	0.030	0.54	51.8	0.806
WTAC-4	409.8	0.143	0.118	0.025	0.58	75.8	0.744
WTAC-5	469.7	0.149	0.123	0.026	0.55	64.4	0.749
WTAC-6	424.2	0.167	0.145	0.022	0.54	96.8	0.674
WTAC-7	421.9	0.164	0.151	0.013	0.54	70.3	0.595
WTAC-8	405.0	0.157	0.148	0.009	0.55	88.4	0.532
WTAC-9	509.6	0.192	0.163	0.029	0.54	93.6	0.729
WTAC-10	430.7	0.169	0.147	0.022	0.54	64.2	0.615
WTAC-11	397.8	0.207	0.177	0.030	0.53	87.5	0.707
WTAC-12	382.5	0.143	0.114	0.029	0.53	60.8	0.763
WTAC-13	377.9	0.148	0.129	0.019	0.54	74.5	0.685
WTAC-14	444.7	0.167	0.140	0.027	0.58	96.4	0.695
WTAC-15	216.4	0.1367	0.113	0.024	0.54	58.3	0.704
WTAC-16	563.2	0.201	0.167	0.034	0.57	106.4	0.723

Figure S1b. It can be seen that the medium size of the micropores was around 0.5 nm, which was close to the size of hydrolyzed K^+ ions (0.331 nm).[26] This indicated that micropores created in the activated carbon samples were good for supercapacitor application. When the size of the micropores is comparable to the ion size, the micropores make maximum contribution to the EDLC due to high electro-adsorption originated from the strong interaction of ions with the pore inwall.[27,28] The specific surface area and the pore structure data are summarized in Table 3. It can be seen that the specific surface area, the total pore volume, and the mesopore/micropore volume ratio can be tuned by adjusting the activation parameters, which will in turn affect the supercapacitor performance. After activation with a H_3PO_4/char ratio of 9 at 840 °C for 2.4 h, the activated carbon sample (WTAC-2) showed the lowest surface area (202 m^2/g) and the lowest pore volume (0.066 cm^3/g). After activation with a H_3PO_4/char ratio of 5 at 900 °C for 3.5 h, the sample (WTAC-16) exhibited the highest specific surface area of 563 m^2/g and highest pore volume of 0.201 cm^3/g. These values were comparable to or even larger than those reported in the literature in which KOH, $ZnCl_2$, or CO_2 were used as the activation agents to produce the activated carbon from waste tire-derived char.[29−33]

The performance of the activated carbon electrodes was first characterized by CV. Herein the specific capacitance (C_S) is defined as the capacitance obtained at the lowest scan rate (2 mV/s) since the long-distance ion diffusion process can be omitted at such a low scan rate. The specific capacitance can be expressed

$$C_S = \frac{\int I\,dt}{Vm} \quad \text{(at 2 mV/s)} \tag{1}$$

where I is the current measured, V is the voltage window (1 V), and m is the mass of a single electrode. The rate capability (R), which is indicative of the power delivery capability of supercapacitor, is defined as the ratio of the capacitance value obtained at 100 mV/s to that at 2 mV/s. R can be expressed as

$$R = \frac{C_{100\text{mV/s}}}{C_{2\text{mV/s}}} \tag{2}$$

dx.doi.org/10.1021/sc500336h | ACS Sustainable Chem. Eng. 2014, 2, 1592−1598

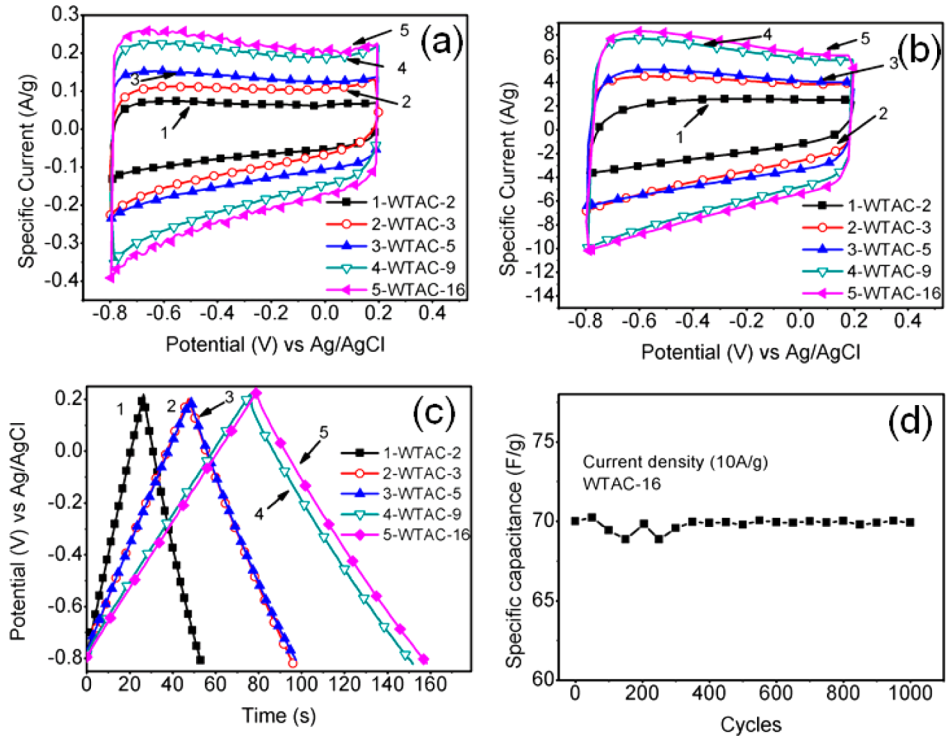

Figure 2. (a) Cyclic voltammetric curves obtained from the activated carbon electrodes at a scan rate of 2 mV/s and (b) at a scan rate of 100 mV/s; (c) charge−discharge curves of the activated carbon electrodes at a current density of 1 A/g; and (d) testing of the stability of the WTAC-16 electrode at 10 A/g for 1000 cycles of charge−discharge.

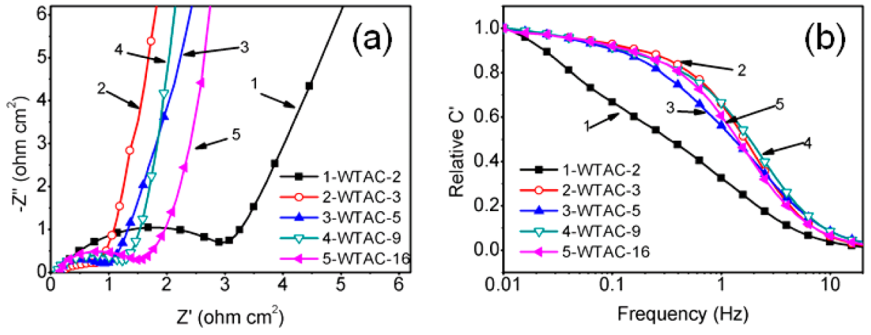

Figure 3. (a) Nyquist plots of the supercapacitors and (b) the corresponding frequency-dependent capacitance response.

Figure 2a shows the CV curves of typical activated carbon electrodes at a scan rate of 2 mV/s. The well-defined EDLC behavior was reflected by the near-rectangular shape of CV curves observed for all the samples. When the scan rate increased to 100 mV/s, the well-defined rectangular shape of CV curves can still be retained for almost all the samples except for WTAC-2 as shown in Figure 2b, which confirmed that the electrodes had good rate capability. The specific capacitance and the rate capability data were also summarized in Table 3.

Constant current charge−discharge measurement was performed to further investigate the electrochemical behavior of the activated carbon electrodes. Figure 2c demonstrates the results obtained at a current density of 1 A/g. The symmetrical triangle shape of the charge−discharge curves confirmed the pure EDLC behavior without any redox reaction involved. The specific capacitances of the WTAC-2, 3, 5, 9, and 16 samples were 26, 47, 49, 76, and 80 F/g, respectively, which were in agreement with the values derived from the CV curves. The WTAC-16 sample was operated under the constant-current charge−discharge condition for 1000 cycles at 10 A/g in order to test the stability of the activated carbon electrode (Figure 2d). The specific capacitance was reduced by only 3% after 1000 cycles, which indicated that the as-synthesized activated carbon electrode can be operated in practice.

Impedance spectra were used to clarify the reason for the difference in the rate capability of WTAC samples. Figure 3a reveals the Nyquist spectra of impedance in the frequency range of 30 kHz ∼ 0.1 Hz. An equivalent circuit can represent the electrochemical cells (Supporting Information Figure S2). The ohmic resistance (R_s), as the interception of the Nyquist spectra with the Z' axis at the high frequency, came from the series resistance of the electrolyte, the contact leads, and the sheet resistance of the carbon film. The ohmic resistance was ∼0.1 Ω·cm^2 for all the samples, which confirmed the good conductivity and high quality of the activated carbon electrodes. The straight line at the low frequency region was characteristic of the supercapacitance (C). The R_cC_c unit represents the semiarc, which appeared at the medium frequency range. It was

dx.doi.org/10.1021/sc500336h | ACS Sustainable Chem. Eng. 2014, 2, 1592−1598

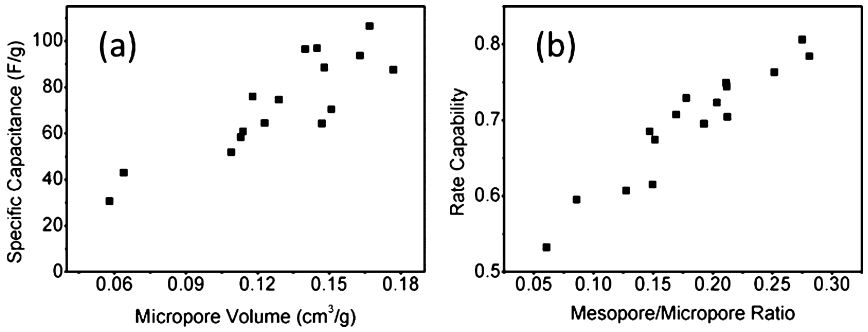

Figure 4. (a) Specific capacitance of the activated carbon electrodes versus the micropore volume and (b) the rate capability versus the mesopore/micropore volume ratio.

ascribed to the charge transfer process at the electrode/electrolyte interface. The diameter of the semiarc can be used to quantitatively analyze the charge transfer resistance (R_c), which becomes significant when a supercapacitor is operated at a high rate. It can be seen that the WTAC-2 sample had the largest charge transfer resistance of ~3 Ω·cm^2 while the charge transfer resistance of WTAC-3 sample was ~1 Ω·cm^2. This explained the fact that the WTAC-2 electrodes had the worst rate capability, which was consisted with the CV results. Furthermore, the frequency-dependent capacitance can be calculated as follows

$$C = \frac{1}{j\omega Z} = \frac{-Z''}{\omega |Z|^2} - j\frac{Z'}{\omega |Z|^2} = C' - jC'' \quad (3)$$

where C' is the real capacitance, which represents the deliverable capacitance of the electrodes. Figure 3b shows that the C' value of WTAC-2 sample that had the slowest capacitive response. For other samples, the frequency responses were similar since there was small difference in the rate capability with each other.

The above-mentioned results show that adjusting the activation parameters can tailor the physical properties such as the specific surface area, total pore volume, micropore volume, and mesopore volume, which can tune the specific capacitance and the rate capability of the EDLC-type activated carbon electrode. Herein we investigate how many physical properties control the specific capacitance and the rate capability and which physical property is a dominant factor in governing the specific capacitance and the rate capability.

For EDLCs made of the activated carbon electrodes, the porosity of the activated carbon governs its energy storage and power delivery capability. The macropores (>50 nm) act as the ion buffering reservoir.[3,7] Micropores (<2 nm in size) serve as the ion traps for energy storage, and mesopores (2−50 nm in size) act as the ion transport pathways, which is crucial to the power delivery.[7,34] Keeping this in mind, the results in Figure 4 and Table 3 are understandable. Figure 4a plots the specific capacitance (C_S) versus the micropore volume, which shows that C_S increased with an increase in the micropore volume. To further confirm this point, the multiple linear regression method was performed to investigate the dependence of C_S upon multiple physical properties (X_1, X_2 X_3, X_4, and X_5) as shown in Table 3. In the effort to model C_S as a function of X_i, X_3 (micropore volume) was selected as the sole significant predictor by the stepwise regression method, and the resulting fitted model is

$$C_S = 1.7 + 550X_3 \quad (4)$$

The quality of a model can be judged by R^2. R^2 is the proportion of variability in C_S, which can be explained by regression on X_3. The R^2 of model 4 is 74.6%, which indicates that model 4 is a good fit. It is worth noting that model 4 excludes X_1 and X_2 although C_S increases with an increase in both the specific surface area (Supporting Information Figure S3) and the total pore volume (Supporting Information Figure S4). The correlation analysis between the factors suggests that both X_1 (specific surface area) and X_2 (total pore volume) are highly correlated with X_3 (micropore volume) with correlation-(X_2, X_3) = 98.0% and correlation(X_1, X_3) = 82.0%, which is the reason why these two factors (X_1 and X_2) are not included in model 4 because X_3 is already included as the predictor. In addition, X_4 (mesopore volume) is not correlated with X_3, and it is excluded by the stepwise regression from the selected model because it does not have a significant impact on the C_S value. As also evident in Supporting Information Figure S5, the specific capacitance had no correlation with the mesopore.

Similarly, by performing stepwise regression of R (rate capability) upon multiple physical properties (X_1, X_2 X_3, X_4, X_4/X_3, and X_5) in Table 3, the final selected model for the rate capability is given as

$$R = 0.486 + 1.15(X_4/X_3) \quad (5)$$

where X_4/X_3 represents the mesopore/micropore volume ratio. The R^2 of model 5 is 89.6%, indicating that the fitted model 5 is of high quality. Figure 4b shows the rate capability versus the volume ratio of mesopores to micropores. It can be found that, as the mesopore/micropore volume ratio increased, the rate capability also increased. The mesopores can effectively transport the electrolyte ions to the micropores throughout the electrode, which is the key to high capacitance retention at a high scan rate.

In addition, linear regression was carried out to investigate the dependence of R (rate capability) upon X_4 (mesopore volume), and the fitted model is

$$R = 0.533 + 7.10X_4 \quad (6)$$

with R^2 being 54.1%, much lower than the R^2 of model 5. By comparing the R^2 of models 5 and 6, we can conclude that X_4/X_3 (mesopore/micropore volume ratio) is a substantially better predictor than X_4 (mesopore volume). This result indicates that we cannot consider the mesopore volume alone to maximize the rate capability. Instead, we must have the mesopore volume match the micropore volume.

In contrast, the stepwise regression results show that the rate capability has no evident correlation with the micropore volume (see Supporting Information Figure S6), the total pore

volume (Supporting Information Figure S7), and the specific surface area (Supporting Information Figure S8) of the activated carbon electrode in this study.

The rate capability of EDLC-based supercapacitor electrodes generally depends on four processes:

(i) Ion diffusion in the liquid electrolyte: The charge storage occurs in the micropores only when the ions can be delivered to the microspores via diffusion in the liquid electrolyte through the mesopores to the micropores. Obviously increasing the mesopore/micropore volume ratio will facilitate the ion diffusion.

(ii) Charge transfer at the electrolyte/electrode interface: In this study, all the samples had almost identical charge transfer resistance (1 $\Omega\cdot cm^2$) except for WTAC-2 (3 $\Omega\cdot cm^2$), which was confirmed by the electrochemical impedance analysis. Therefore, a high charge transfer resistance was one reason for a low rate capability of the WTAC-2 sample.

(iii) Ion adsorption on the surface of solid electrode: The ion adsorption is affected by the surface chemistry and the surface charge of solid electrode as well as the diameter of micropores, which controls the solvation of ions. All the samples in this study had almost the same surface chemistry, surface charge, and micropore diameter. Hence the ion adsorption process was not the dominant factor that led to variation of the rate capability among all the samples.

(iv) Electron transport in the solid electrode and in the whole circuit: All the samples were highly conductive, which was reflected by the low ohmic resistance (0.1 $\Omega\cdot cm^2$) derived from the electrochemical impedance analysis. Hence the electron transport process was not a rate-limiting factor for the power delivery in this study.

On the basis of the above analysis, it is not surprising that the volume ratio of mesopores to micropores was the dominant factor that governed the rate capability of the activated carbon electrodes. The WTAC-2 sample showed the lowest rate capability because it had the lowest mesopore/micropore volume ratio while the WTAC-3 and WTAC-16 samples exhibited higher rate capability due to their higher mesopore/micropore volume ratio. The lowest specific capacitance (C_S) was observed for the WTAC-2 sample because it had the lowest micropore volume, total pore volume, and specific surface area. In contrast, the WTAC-16 sample exhibited the highest specific capacitance, which exceeded 100 F/g. This value was comparable to that obtained from the activated carbon electrodes derived from coffee waste, coconut shells and bamboo.[12]

Finally, the activation process in Table 2 affected the physical properties (Table 3) of the activated carbon. Hence the activation process controlled the performance of activated carbon electrodes. A statistical model was developed to correlate the specific capacitance (or rate capability) with the activation variables including the H_3PO_4/char ratio (ratio), the activation temperatures (T, °C), and the activation time (t, hour) as follows:

$$C_S = -7432 + 15.6T - 0.07\text{ratio} + 281t - 0.311Tt - 0.00807T^2 \quad (7)$$

$$R = 24.0 - 0.0455T - 0.347\text{ratio} - 1.33t + 0.000353T\,\text{ratio} + 0.00141Tt + 0.000022T^2 \quad (8)$$

According to eq 7, increasing the H_3PO_4/char ratio (ratio) reduces C_S because a higher H_3PO_4 content results in a higher activation degree, which reduces the micropore volume. At a given temperature (T), prolonging the activation time (t) also reduces C_S. When t is fixed, increasing T increases the rate capability (R) because a higher activation degree results in a larger level of mesopores. These fitting trends were consistent with the experimental results.

Besides the pore structure, other factors such as the chemical composition and the chemical structure were examined. The chemical compositions of the selected activated carbon samples are listed in Table S1 in the Supporting Information. Also, the Raman spectra of the activated carbon samples are shown in Figure S9 in the Supporting Information. The oxygen content in the activated carbon samples varied from 4.7 to 11.7 at %. The activated carbon samples also contained a small amount of N, S, P, and Si. The Raman spectra displayed the D band and the G band. The G band was ascribed to the in-plane vibration of sp^2 carbon atoms while the D band was attributed to the sp^3 carbons. The intensity ratio of the D band to the G band varied from 0.65 to 0.83. The statistical analysis of our experimental data showed that both the specific capacitance and the rate capability possessed negligible correlation with the impurities and the intensity ratio of the D band to the G band.

CONCLUSIONS

In summary, the activated carbon electrodes were successfully prepared using waste tires as the precursor. The H_3PO_4 activation process effectively generated a porous structure in the carbon materials. The specific surface area, the total pore volume, the mesopore volume, and the micropore volume can be tailored by adjusting the activation parameters. The results from the statistical multiple linear regression and stepwise regression methods clarified the correlation of the specific capacitance and the rate capability with the physical properties of the activated carbon electrode. The specific capacitance was mainly controlled by the micropore volume of the activated carbon electrode; and it is not correlated to the mesopores volume. The rate capability has no evident correlation with the micropore volume, the total pore volume, and the specific surface area. Actually it is dominated by the mesopore/micropore volume ratio instead of the absolute value of mesopore volume. This result indicates that the mesopore volume cannot be considered alone to maximize the rate capability. Instead, the mesopore volume must match the micropore volume. Generally, the rate capability of EDLC-based supercapacitor electrodes depends on four processes: (i) ion diffusion in the liquid electrolyte, (ii) charge transfer at the electrolyte/electrode interface, (iii) ion adsorption on the surface of solid electrode, and (iv) electron transport in the solid electrode and in the whole circuit. For the samples studied here, ion diffusion in the liquid electrolyte is the rate-limiting factor for the rate capability of activated carbon electrode. Finally, the best EDLC-type supercapacitor electrode exhibited a specific capacitance of 106 F/g.

ASSOCIATED CONTENT

Supporting Information

Detailed materials characterization results (BET, XPS, FTIR, and Raman) and additional analysis of the electrochemical performance of the activated carbon with the pore structures. This material is available free of charge via the Internet at http://pubs.acs.org/.

AUTHOR INFORMATION

Corresponding Author

*Fax: +1-304-293-6689. E-mail: nick.wu@mail.wvu.edu.

Notes

The authors declare no competing financial interest.

ACKNOWLEDGMENTS

F.Y. is grateful for partial support by NSF grant (CMMI-1068131). The use of the WVU Shared Facility is appreciated. The authors thank Mr. J. Bright, S. Hao, and P. Zheng for their assistance with XPS, Raman, and FTIR analysis.

REFERENCES

(1) Eberle, U.; Helmolt, R. Von. Sustainable transportation based on electric vehicle concepts: a brief overview. *Energy Environ. Sci.* **2010**, *3*, 689−699.

(2) Wang, G. P.; Zhang, L.; Zhang, J. J. A review of electrode materials for electrochemical supercapacitors. *Chem. Soc. Rev.* **2012**, *42*, 797−828.

(3) Simon, P.; Gogotsi, Y. Materials for electrochemical capacitors. *Nat. Mater.* **2008**, *7*, 845−854.

(4) Winter, M.; Brodd, R. J. What are batteries, fuel cells, and supercapacitors? *Chem. Rev.* **2004**, *104*, 4245−4269.

(5) Jayalakshmi, M.; Balasubramanian, K. Simple capacitors to supercapacitors - an overview. *Int. J. Electrochem. Sci.* **2008**, *3*, 1196−1217.

(6) Zhao, X.; Sánchez, B. M.; Dobson, P. J.; Grant, P. S. The role of nanomaterials in redox-based supercapacitors for next generation energy storage devices. *Nanoscale* **2011**, *3*, 839−855.

(7) Zhi, M. J.; Xiang, C. C.; Li, J.; Li, M.; Wu, N. Q. Nanostructured carbon-metal oxide composite electrodes for supercapacitors: a review. *Nanoscale* **2013**, *5*, 72−88.

(8) Zhi, M.; Manivannan, A.; Meng, F.; Wu, N. Q. Highly conductive electrospun carbon nanofiber/MnO_2 coaxial nano-cables for high energy and power density supercapacitors. *J. Power Sources* **2012**, *208*, 345−353.

(9) He, X.; Zhao, N.; Qiu, J.; Xiao, N.; Yu, M.; Yu, C.; Zhang, X.; Zheng, M. Synthesis of hierarchical porous carbons for supercapacitors from coal tar pitch with nano-Fe_2O_3 as template and activation agent coupled with KOH activation. *J. Mater. Chem. A* **2013**, *1*, 9440−9448.

(10) He, X.; Li, R.; Qiu, J.; Xie, K.; Ling, P.; Yu, M.; Zhang, X.; Zheng, M. Synthesis of mesoporous carbons for supercapacitors from coal tar pitch by coupling microwave-assisted KOH activation with a MgO template. *Carbon* **2012**, *50*, 4911−4921.

(11) Raymundo-Pinero, E.; Gao, Q.; Beguin, F. Carbons for supercapacitors obtained by one-step pressure induced oxidation at low temperature. *Carbon* **2013**, *61*, 278−283.

(12) Lu, W.; Gleb, Y. Nanostructured activated carbons from natural precursors for electrical double layer capacitors. *Nano Energy* **2012**, *1*, 552−565.

(13) Titirici, M.; White, R.; Falco, C.; Sevilla, M. Black Persperctives for a green future: hydrothermal carbon for environmental protection and energy storage. *Energy Environ. Sci.* **2012**, *5*, 6796−6822.

(14) Lee, B.; Lee, Y. S.; Misra, R.; Renganathan, N. G. Recycled waste paper-A new source of raw material for electric double-layer capacitors. *J. Power. Sources* **2009**, *190*, 587−592.

(15) Rufford, T. E.; Hulicova-Jurcakova, D.; Fiset, E.; Zhu, Z.; Lu, G. Q. Double-layer capacitance of waste coffee ground activated carbons in an organic electrolyte. *Electrochem. Commun.* **2009**, *11*, 974−977.

(16) Markets and Uses for Scrap Tires, US EPA. http://www.epa.gov/wastes/conserve/materials/tires/ (accessed Feb 3, 2014).

(17) Fung, P. P. M.; Cheung, W. H.; McKay, G. Systematic analysis of carbon dioxide activation of waste tire by factorial design. *Chin. J. Chem. Eng.* **2012**, *20*, 497−504.

(18) Edward, L. K.; Mui, D.; Ko, C. K.; McKay, G. Production of active carbons from waste tyres- a review. *Carbon* **2004**, *42*, 2789−2805.

(19) Suuberg, E. M.; Aarna, I. Porosity development in carbons derived from scrap automobile tires. *Carbon* **2007**, *45*, 1719−1726.

(20) Shah, J.; Jan, M. R.; Mabood, F.; Shahid, M. Conversion of waste tyres into carbon black and their utilization as adsorbent. *J. Chin. Chem. Soc.* **2006**, *53*, 1085−1089.

(21) Helleur, R.; Popovic, N.; Ikura, M.; Stanciulescu, M.; Liu, D. Characterisation and potential applications of pyrolytic char from ablative pyrolysis of used tires. *J. Anal. Appl. Pyrol.* **2001**, *58−59*, 813−824.

(22) Lehmann, C. M.; Rostam-Abadi, B. M.; Rood, M. J.; Sun, J. Reprocessing and reuse of waste tire rubber to solve air-quality related problems. *Energy Fuels* **1998**, *13*, 1095−1099.

(23) Roussak, O. V.; Gesser, H. D. *Applied Chemistry*; Springer: New York, 2013.

(24) Burke, A.; Miller, M.; Parker, N. *Ultracapacitor technology: present and future performance and applications*; Nesscap Co., Ltd., 2006.

(25) Betancur, M.; Martinez, J. D.; Murillo, R. Production of activated carbon by waste tire thermochemical degradation with CO_2. *J. Hazard. Mater.* **2008**, *168*, 882−887.

(26) Volkov, A.; Paula, S.; Deamer, D. Two mechanisms of permeation of small neutral molecules and hydrated ions across phospholipid bilayers. *Bioelectrochem. Bioenerg.* **1997**, *42*, 153−160.

(27) Yamada, H.; Nakamura, H.; Nakahara, F.; Moriguchi, I.; Kudo, T. Electrochemical study of high electrochemical double layer capacitance of ordered porous carbons with both meso/macropores and micropores. *J. Phys. Chem. C* **2007**, *111*, 227−233.

(28) Bae, J. H.; Han, J. H.; Chung, T. D. Electrochemistry at nanoporous interfaces: new opportunity for electrocatalysis. *Phys. Chem. Chem. Phys.* **2012**, *14*, 448−463.

(29) Teng, K.; Lin, Y.; Hsu, L. Production of activated carbons from pyrolysis of waste tires impregnated with potassium hydroxide. *J. Air & Waste Manage. Assoc.* **2000**, *50*, 1940−1946.

(30) Sun, J.; Brady, T.; Rood, M.; Lehmann, C. M.; Rostam-Abadi, A. Adsorbed natural gas storage with activated carbons made from Illinois coals and scrap tires. *Energy Fuels* **1997**, *11*, 316−322.

(31) Suuberg, E. M.; Aarna, I. Porosity development in carbons derived from scrap automobile tires. *Carbon* **2007**, *45*, 1719−1726.

(32) Sainz-Diaz, C.; Griffiths, A. Activated carbon from solid wastes using a pilot-scale batch flaming pyrolyser. *Fuel* **2000**, *79*, 1863−1871.

(33) Helleur, R.; Popovic, N.; Ikura, M.; Stanciulescu, M.; Liu, D. Characterisation and potential applications of pyrolytic char from ablative pyrolysis of used tires. *J. Anal. Appl. Pyrol.* **2001**, *58−59*, 813−824.

(34) Liu, C.; Li, F.; Ma, L. P.; Cheng, H. M. Advanced materials for energy storage. *Adv. Mater.* **2010**, *22*, E28−E62.